Published in final edited form as:
Eur J Neurosci. 2013 April ; 37(7): 1090–1102. doi:10.1111/ejn.12119.

Motor cortex electrical stimulation promotes axon outgrowth to brain stem and spinal targets that control the forelimb impaired by unilateral corticospinal injury

Jason B. Carmel[1,2,3], **Hiroki Kimura**[3], **Lauren J. Berrol**[3], and **John H. Martin**[3,4,5]

[1]Department of Neurology and Neuroscience, Weill Cornell Medical College, New York, NY 10021

[2]Burke-Cornell Medical Research Institute

[3]Department of Physiology, Pharmacology and Neuroscience, City College of the City University of New York, New York 10031

[4]Departments of Neuroscience, Neurological Surgery, and Psychiatry, Columbia University, New York, New York 10032

[5]N.Y.S. Psychiatric Institute, New York, New York 10032

Abstract

We previously showed that electrical stimulation of motor cortex (M1) after unilateral pyramidotomy in the rat increased corticospinal tract (CST) axon length, strengthened spinal connections, and restored forelimb function. Here, we tested: 1) if M1 stimulation only increases spinal axon length or if it also promotes connections to brain stem forelimb control centers, especially magnocellular red nucleus; and 2) if stimulation-induced increase in axon length depends on whether pyramidotomy denervated the structure. After unilateral pyramidotomy, we electrically stimulated the forelimb area of intact M1, to activate the intact CST and other corticofugal pathways, for 10 days. We anterogradely labeled stimulated M1 and measured axon length using stereology. Stimulation increased axon length in both the spinal cord and magnocellular red nucleus, even though the spinal cord is denervated by pyramidotomy and the red nucleus is not. Stimulation also promoted outgrowth in the cuneate and parvocellular red nuclei. In the spinal cord, electrical stimulation caused increased axon length ipsilateral, but not contralateral, to stimulation. Thus, stimulation promoted outgrowth preferentially to the sparsely corticospinal-innervated and impaired side. Outgrowth resulted in greater axon density in the ipsilateral dorsal horn and intermediate zone, resembling the contralateral termination pattern. Importantly, as in spinal cord, increase in axon length in brain stem also was preferentially directed towards areas less densely innervated by the stimulated system. Thus, M1 electrical stimulation promotes increases in corticofugal axon length to multiple M1 targets. We propose the axon length change was driven by competition into an adaptive pattern resembling lost connections.

Corresponding authors: Jason B. Carmel, MD, PhD, Burke-Cornell Medical Research Institute, 785 Mamaroneck Avenue, White Plains, NY 10605, Tel: 914-368-3135, jbc7001@med.cornell.edu, John H. Martin, Ph.D., Department of Physiology, Pharmacology & Neuroscience, City College of the City University of New York, 160 Convent Avenue, New York, NY 10031, Tel: 212-650-5956, jmartin@ccny.cuny.edu.

The authors have no conflicts of interest.

Keywords

Corticospinal; electrical stimulation; injury; recovery; motor cortex; rat

INTRODUCTION

Strengthening spared connections from motor cortex (M1) after brain or spinal cord injury has emerged as an important strategy for motor system repair (Hagg, 2006; Jankowska & Edgley, 2006). Corticospinal tract (CST) axons sprout after partial lesion, and sprouting is augmented with electrical stimulation (Brus-Ramer et al., 2007). Importantly, activity promotes recovery after unilateral pyramidotomy, either with electrical stimulation of the intact M1 (Carmel et al., 2010) or forced use of the impaired limb (Maier et al., 2008).

We had two goals in this study. Our first goal was to determine, in animals with unilateral pyramidotomy, which targets of M1 have the greatest increase in innervation after M1 stimulation, and, therefore, might contribute to motor recovery. We considered three possibilities. First, sprouting of ipsilateral CST connections, as seen in previous studies (Maier et al., 2008; Carmel et al., 2010) could allow M1 to control spinal circuits directly. Second, M1 could exert control via the red nucleus, especially the magnocellular portion, which projects to the spinal cord in an overlapping manner with the CST. Third, stimulation could promote corticofugal connections to somatic sensory processing regions—both in the spinal cord dorsal horn and in the cuneate nucleus. These could enable new feedback control strategies for skill learning (Ghosh et al., 2009). We measured corticofugal axon length in the spinal cord, red nucleus, and cuneate nucleus emanating from M1 on the intact side (see Fig. 1A). We reasoned that if outgrowth only occurred at the spinal level, then this would emphasize the importance of direct CST connections and deemphasize indirect pathways.

Our second goal was to understand the rules governing local changes in length of stimulated axons after injury. We have shown that activity strongly sculpts corticofugal connections during development (Martin et al., 1999; Martin et al., 2009); stimulated cortical axon terminations increase in length because they outcompete their neighbors. We hypothesized competition within the stimulated system that would drive M1 innervation towards areas of sparse CST terminations after unilateral pyramidotomy. We also considered competition between the stimulated M1 and projections from the other M1 above the site of pyramidotomy. Such competition might result in more robust increases in axon length in regions denervated by pyramidotomy (see Fig. 1A; the spinal cord and cuneate nucleus) than areas that were not denervated (red nucleus). We tested these ideas using stereological sampling, which allows quantification of sparse and dense terminations alike.

Stimulation produced increases in axon length from spared CST axons to spinal cord and red nucleus, suggesting that stimulation recruits both direct and indirect spinal motor pathways, as well as to the cuneate nucleus, which may reflect novel somatic sensory regulation. Our results are consistent with activity-dependent competition within the stimulated system, but not between projections of each M1. Further, stimulation promoted outgrowth in the ipsilateral dorsal horn and intermediate zone, resembling the crossed CST pattern. We propose that stimulation-induced increase in axon length is sensitive to local competition between stimulated terminations, and this mechanism could help restore adaptive circuits after injury.

MATERIALS AND METHODS

Overview

We used stereological methods to quantify how electrical stimulation affected axonal connections from M1 to subcortical targets integral to forelimb motor control—the spinal cord, red nucleus and cuneate nucleus—after pyramidotomy on the other side (Fig. 1A). We implanted an electrode over the forelimb area of M1 before cutting the pyramid opposite to the electrode in all rats (Fig 1B). In rats with injury and stimulation but not rats with injury only we delivered electrical stimulation daily for 10 days, beginning the day after pyramidotomy. On day 31 or 32 after injury, we injected biotinylated dextran amine (BDA) to anterogradely label the corticofugal projections from the intact M1. Twelve days later, rats were killed and the cervical spinal cord, red nucleus and cuneate nucleus were cut in cross section. We visualized corticofugal axons within local regions of the gray matter of the target and measured them using a stereological estimate of axon length. We compared axon length and distribution of axons between rats with injury and stimulation and rats with injury only for each of the corticofugal targets.

Surgical

Experiments were conducted on adult female Sprague Dawley rats (weight 225–275g; Charles River). A total of 17 rats were used for this study. Ten of these rats were used in our previous study(Carmel et al., 2010) but, for the present study, an entirely new set of analyses was conducted. Animals were added because the scope of the present study was broader; axon terminations in some targets could not be counted due to tissue damage, poor BDA visualization, or inappropriate plane and level of sectioning. Thus, although there is large overlap of animals in each group, they are not identical. Figure 1C shows which of the 16 animals were used for each corticofugal target. One additional control animal was used to determine that pyramidotomy fully denervates the cuneate nucleus and does not denervate the red nucleus (data not shown). The surgeries (electrode implantation, pyramidal lesion, and axon tracing) were performed under general anesthesia (90 mg/kg ketamine; 10 mg/kg xylazine, via intraperitoneal injection) and aseptic conditions. All procedures were approved by the institutional animal care and use committees of Columbia University, the New York State Psychiatric Institute, and City College of the City University of New York. All experiments comply with NIH guidelines on the care and use of laboratory animals.

Electrode implantation and stimulation

Briefly, rats were anesthetized and head fixed in a stereotactic frame (David Kopf Instruments, Tujunga, California, USA). We made a craniotomy over the forelimb area of motor cortex. Two stainless steel stimulating electrodes (0.005 inch insulated stainless steel; Plastics One, Roanoke, Virginia, USA) attached to a connector were placed over the dura mater. The wires were bent into an “L” shape with the bottom of the L deinsulated. Wires were run parallel 1.5 mm apart and 4 mm long. We placed the wires over forelimb area of motor cortex: the anterior-posterior position of the angle of the L-shaped electrodes was in line with bregma, and the lateral positions were 2 mm and 3.5 mm, respectively (see Fig. 4A, inset). The electrodes extended anterior from bregma to 4mm anterior to bregma, which covers the caudal forelimb area of M1(Brus-Ramer et al., 2009). To confirm proper placement, we used a constant current stimulator (A-M Systems, Sequim, Washington, USA) to deliver trains of stimuli (0.2 ms duration, 333 Hz, 45 ms, every 2 seconds) in order to provoke a movement. We adjusted the current to the minimal value to evoke contralateral forelimb movements, which was typically 1.1–1.8 mA. It should be noted that these high currents likely reflect the epidural position of the electrode. Nevertheless, they were selective for the forelimb motor cortex (see below). We secured the electrodes using microscrews (PlasticsOne) and dental acrylic cement. We placed stimulating electrodes at

least 1 week before CST injury and determined that electrode placement caused no injury, as determined by change in motor performance (data not shown) and histology. To verify that chronic epidural stimulation did not injure M1 underlying the dura mater, we examined the brains of 3 rats with chronic cortical stimulation. We cut coronal sections of M1 underlying the electrodes at 40μm. Sections were Nissl-stained to examine changes in cellular architecture. We also examined the tissue for evidence of astrogliosis by staining for the glial acidic fibrillary protein (GFAP; Sigma #G3893, 1:400 visualized by peroxidase labeled anti-mouse IgG; Vector #PI-2000, 1:200). We visualized all tissue sections with Olympus BX60 microscope and Optronics Microfire Digital Microscope Camera, Goleta, California, USA).

Beginning the day after pyramidotomy, we stimulated rats 6 hours daily for 10 days. For electrical stimulation, the connector on the rats' heads was attached to a commutator (Plastics One) mounted to the top of the cage, and trains of stimuli (described above) were given at the threshold to provoke a contralateral forelimb motor response on each trial. The motor response was limited to the forelimb contralateral to stimulation, and usually consisted of digit flexion, wrist extension, or elbow flexion. We never observed hind limb or ipsilateral movements at these threshold currents. Rats were given stimulation at the initial motor threshold for a 6-hour period during the day. Rats ate and drank during the stimulation, but mostly they slept since they are nocturnal. They never pawed at their heads or showed any signs of pain or distress. Motor responses were absent while rats slept or bore weight on the forelimbs. However, the responses returned when the rat was weight-supported and the forelimb allowed to hang freely.

Pyramidotomy

Rats were anesthetized, as described above, placed supine in head fixation, and the pyramids exposed. One pyramid was completely transected at the rostral medulla using iridectomy scissors and a second pass with a microknife. Lesions were examined using Kluver–Barrera staining (Fig 1B1; Kluver and Barrera, 1953) or dark-field microscopy of the medulla at the site of injury (Carmel et al., 2010). Figure 1B2 demonstrates the minimum (black) and maximum (gray) lesion size. Lesions were confirmed to be histologically complete without extension into adjacent structures.

Anterograde labeling of corticofugal axons

On day 31 or 32 after pyramidotomy, we injected biotinylated dextran amine (BDA; 10%, Life Technologies, Grand Island, New York, USA) into the forelimb area of motor cortex to anterogradely label the intact corticofugal system. In the one control animal we injected BDA into the motor cortex ipsilateral to the pyramidal lesion to determine if this resulted in loss of corticorubral projections (see below). Briefly, after inducing anesthesia, we removed the stimulating electrode and incised the dura mater to expose the cortical surface. We made 15 injections (300 nl each) at a depth of 1.5mm throughout the forelimb area of motor cortex. After 12 days, rats were given an anesthetic overdose and perfused through the heart with heparanized saline followed by 4% paraformaldehyde. The brain and spinal cord were removed, postfixed in the same fixative at room temperature for 2 hours, and then transferred to 20% sucrose in 0.1 M phosphate buffer at 4°C overnight. Transverse sections of the sixth cervical section were cut at 40μm and processed for BDA. For visualization of BDA, sections were incubated in PBS, pH 7.4, containing 1% avidin–biotin complex reagent (ABC kit; Vector Laboratories, Burlingame, California, USA) and 0.2% Triton X-100 (Sigma) for 2 h at room temperature. After rinsing, sections were incubated with the chromogen diaminobenzidine (DAB; Sigma) for 6–30 min. After rinsing again, sections were mounted on gelatin-coated slides, air dried overnight, dehydrated, and coverslipped.

Three lines of evidence suggest it is unlikely that stimulation affected anterograde transport. First, tracer is injected three weeks after stimulation is complete. Second, the number of tracer-labeled axons in the main corticospinal tract was not different between the injury only and injury plus stimulation groups. Finally, differences in tracer efficiency would not explain the differences in topographic distribution of the tracer.

Identification of magnocellular red nucleus and cuneate nucleus

We identified the red nucleus and cuneate nucleus using darkfield microscopy. To insure accurate tracing of the red nucleus under darkfield conditions, we injected Fluorogold (FG, 5%; Fluorochrome, Denver, Colorado, USA) into the gray matter of the cervical spinal cord to retrogradely the magnocellular portion of the red nucleus within a subset of animals (n=3). Briefly, after inducing anesthesia and injecting BDA as above, we exposed the C6 segment of spinal cord and injected 1μl of 5% FG at 0.8mm lateral and 1.5mm deep on each side of the spinal cord. After FG injections, rats developed difficulty walking around the cage and could not easily rear by the end of the survival period, presumably due to the toxicity of the tracer (He, 2009). But they ate, drank, and urinated independently. Animals were killed 12 days later. For these 3 animals, we traced the red nucleus under both darkfield (Fig. 2A1) and fluorescence (2A2), and we compared the area of the contours for consistency. FG-labeled neurons filled more than half of the red nucleus as measured by darkfield microscopy (data not shown) and fell within the darkfield boundary. This indicates that darkfield identification of the red nucleus allowed full measurement of corticofugal terminations into the region of magnocellular neurons, which give rise to the rubrospinal tract. The parvocellular red nucleus had sparser retrograde label. Based on this analysis and with the help of local tissue markers, we were able to discriminate confidently which red nucleus sections were magnocellular and which were parvocellular. In addition, the boundaries of the red nucleus were very reproducible between subjects, as shown by overlaying the drawn boundary from each parvocellular red nucleus (Fig. 2A3). The location of analyzed red nucleus sections was approximately 5.4 to 6.0mm caudal to bregma (Paxinos & Watson, 1986).

The cuneate nucleus is easily identified lateral to the gracile nucleus because it is surrounded by white matter (Fig. 2B). The nucleus is traced under darkfield illumination (2B1). We addressed any concerns about the boarder of the cuneate nucleus by staining adjacent sections with Kluver-Barrera (2B2). We analyzed the densely labeled areas of the nucleus, which corresponds to the level of area postrema, where the pyramids had begun to flatten just rostral to decussating, and the twelfth nerve root was visible—approximately 14mm caudal to bregma(Paxinos & Watson, 1986).

Axon length estimation

We measured corticofugal axon length within the red nuclei, cuneate nuclei, and spinal cord using the “spaceballs” probe in the Stereo Investigator stereology program (MBF Bioscience, Williston, Vermont, USA). After we traced the area of interest—the gray matter of the spinal cord, the red nucleus, or the cuneate nucleus—the program places virtual spheres (“space balls”) within the tissue. At 1000x magnification (oil immersion), we marked intersections between the virtual sphere and labeled axons within the gray matter. An intersection is defined as contact or crossing of the linear axon and the cross section of the sphere, a circle of varying diameter (Fig. 3A3, red arrows). We used the number of interactions to compute an associated axon length (Mouton et al., 2002). Note, this produces an axon length within the volume defined by the area of the contour outlining the structure of interest and the 40μm thickness of the section. This measurement allows us to compare the magnitude and two-dimensional location of axon length accurately.

This method of measuring axon length has two principal benefits. First, it allows comparisons between low-density areas, which we previously measured with hand tracings(Brus-Ramer *et al.*, 2007; Friel & Martin, 2007) and high-density areas, in which hand tracing is practically impossible. Importantly, the ability to generate accurate estimates in low- and high-density regions allows comparisons across different corticofugal targets. Second, stereological sampling allows accurate measures of local axon length. This allows us to determine how stimulation affects outgrowth within the target and to make assertions about highly localized effects.

Our axon length estimates were corrected for the variability in tracing between animals using the average number of BDA-labeled axons within the CST. For the spinal cord, we based the correction factor on the number of BDA-labeled axons in the base of the dorsal column opposite the side of M1 injection. We estimated axon number using a different stereological probe, the Optical Disector probe (Stereo Investigator), also at 1000x magnification. The number of dorsal column axons was measured in the same 5 sections in which the gray matter axon length was measured; these numbers were averaged for each rat. The average for each rat was then divided by the average for all rats in this study to generate the correction factor; this was done to keep the axon length as close as possible to the original estimate. The correction factor for each individual rat was then applied to the estimated axon length for that rat to create an axon length adjusted for efficacy of BDA label. For axon length within the cuneate nucleus, the number of BDA-labeled axons in the pyramid at the level of the olivary complex, was estimated, again using the Optical Disector program. For the red nucleus, we considered applying the same methods that we used for the pyramid counts to the peduncle, where the main CST runs. However, axons reach the red nucleus from a dorsomedial trajectory. Thus, we used the number of midline axons (described in the next section) as the correction factor. As described in the Results, the number of midline axons in the red nucleus was not different between rats with injury only and rats with injury and stimulation. In addition, correcting axon length with estimates of CST axons in the peduncle versus the number of midline axons gave nearly identical results in terms of the effect of stimulation (average magnitude of stimulation effect was 2.8 for peduncle correction versus 3.3 for midline axon correction, paired t-test, P=0.19) and variability (average coefficient of variation was 0.72 versus 0.54, paired t-test, P=0.13). For the spinal cord, we measured axon length in five nonadjacent sections per animal. For both the red nucleus and the cuneate nucleus, we used two sections per animal. At the spinal cord and red nucleus, 6 rats with injury only were compared to six rats with injury and stimulation. For the magnocellular and parvocellular red nucleus, five rats with injury only were compared with five rats with injury and stimulation. The overlap of animals used for each analysis is shown in Figure 1C.

Regional axon length analysis

We represented corticofugal axon innervation of all targets using color-coded density maps and additionally for the spinal cord, a line graph of axon density along the dorsoventral axis (dorsoventral plot, see Fig. 6D). We started with a map of interactions between axons (the total length of which we estimated) and our stereological probe (the space ball; Fig. 3B). These maps show the interactions as dots; the number of dots is proportional to the local axon length. We corrected interaction maps of individual sections for orientation and aligned with one another according to local tissue features before exporting the images to MATLAB (MathWorks, Natick, Massachusetts, USA). We used custom scripts within MATLAB to overlay interaction maps, correct each for density of labeling, and determine axon length within 40μm by 40μm regions of interest. Thus, MATLAB converts the dots of interactions (Fig. 3B) into a heat map that represents the length of axon within each region of interest (Fig. 3C). Length is represented according to a color scale, from the shortest (blue) to the

longest (red) with the associated numbers indicating an estimate of true (not relative) axon length. Areas without labeling are coded dark blue. We used the same data to construct a dorsoventral plot using a custom program within MATLAB, as previously described (Brus-Ramer *et al.*, 2007; Friel & Martin, 2007).

The shape of the spinal cord gray matter at each spinal level is consistent between animals. However, to ensure that axon density changes are due to electrical stimulation, not different gray matter shapes, we warped individual sections from each animal to match a template(Watson et al., 2009) using the program Morpheus Photo Warper (Morpheus Software, Indianapolis, Indiana, USA).

Crossing axon analysis

The number of axons crossing the midline at the level of the red nucleus and the spinal cord was estimated using our previously published method (Brus-Ramer et al., 2007). Briefly, the same sections used to estimate axon length were visualized using differential interference contrast microscopy at 400x. Dorsoventrally oriented lines were drawn at midline and a parallel line drawn 25μm lateral to midline on the ipsilateral hemifield using the Neurolucida program (MBF Bioscience). In the spinal cord, the number of midline axons within the midline spinal cord gray matter was counted. In the red nucleus, midline axons between the dorsal limit and ventral limit of the two nuclei were counted. Since cortico-cuneate axons likely decussate in the main pyramidal decussation before projecting dorsally to the cuneate nucleus, the number of crossing axons cannot be counted.

Statistics

Statistical analyses were performed using an unpaired Student's t-test in Excel (Microsoft). To correct for multiple comparisons, we applied the False Discovery Rate (FDR, SAS software 9.3, Cary, North Carolina, USA), which applies a progressively more stringent cutoff for significance with each pairwise comparison (Storey, 2002). FDR, widely used among statisticians, fits with the intention of multiple comparisons correction, that each additional test presents an increased risk of a type 1 error, e.g. finding differences between groups due to chance. We compared animals with injury to those with injury and stimulation at four anatomical locations (spinal cord, cuneate nucleus, magnocellular red nucleus; parvocellular red nucleus) and on both sides. This resulted in 8 comparisons. We express each of the pairwise t-tests as raw p values followed by the p value corrected for multiple comparisons with FDR. To look for outliers, we plotted our data with box plots (Kaleidograph 3.6, Synergy Software, Reading, Pennsylvania, USA); there were no outliers.

RESULTS

Chronic epidural M1 stimulation does not produce gliosis

To determine if epidural stimulation of M1 at current sufficient to provoke a contralateral forelimb movement (1.1–1.8mA) damaged M1, we examined coronal sections under the electrodes (Fig 4, inset indicates plane of section, red arrows indicate approximate location of stimulating electrodes). Staining for GFAP (Fig 4A) revealed similar similar staining patterns and levels in the unstimulated (4A1) and stimulated (4A2) sides . Similarly, Nissl-stained sections (Fig. 4B) demonstrated similar cellular architecture in unstimulated (4B1) and stimulated (4B2) M1.

M1 stimulation drives outgrowth to the spinal cord and preferentially targets the impaired side

We used an unbiased estimate of axon length within gray matter (see Methods) to compare corticofugal outgrowth in rats with unilateral pyramidotomy alone or injury and chronic

electrical stimulation of M1 on the intact side (see Fig. 1A). This allowed us to compare preterminal and terminal axon length in gray matter across different targets within the brain stem and spinal cord whether those structures were densely or sparsely innervated. For the spinal cord, we measured labeled CST axons within the C6 segment. We tested the hypothesis that electrical stimulation of M1 on the intact side would produce the greatest increase in axon length in the impaired half of the spinal cord (Fig. 5A, red), where terminations are sparse (less competition within the stimulated system) and where all CST terminations from the other side were lost with pyramidotomy (no competition from normally dense connections from the other M1).

Figure 5B shows representative images of BDA-stained C6 spinal cord from one individual with injury only (B1) and an individual with injury and stimulation. We also hand traced all BDA-labeled axons at 400x (Fig. 5D); the tracings are below the photomicrograph of the same 40μm section pictured in 5B. On the dense contralateral side of the spinal cord, there is a larger amount of BDA-labeled axon in the rat with injury and stimulation (5B1) compared with the rat with injury alone (5B2). This stimulation-induced outgrowth (5D2) is particularly obvious dorsal and ventral to the deep dorsal horn, where axons are dense in rats with injury only. Outgrowth is even more striking on the ipsilateral half of the spinal cord. Whereas the ipsilateral axons are very sparse in the rat with injury only (5B1 and 5D1), they are much denser and more widely spread in the rat with injury and stimulation (5B2 and 5D2).

For quantification of axon length, we examined interactions of our stereological probe with BDA-labeled axons at 1000x (Fig 3A3), which allowed unambiguous identification of these interactions. Average total CST axon lengths, corrected for tracer efficiency, are presented in Figure 5C. Expressed as a ratio, stimulation produced a substantially larger increase in axon length in the sparsely innervated ipsilateral side (left set of bar graphs, 4.6-fold change), with a smaller increase on the contralateral half of the spinal cord (right, 2.3-fold change). There also was a substantial increase in absolute axon length bilaterally. Ipsilateral to M1 stimulation, the axon length in animals with injury and stimulation was 8,319 ± 2,287μm, and that of animals with injury only was 1,827 ± 197μm (t-test P=0.009; corrected for multiple comparisons, P=0.014). Contralateral to M1 stimulation, axon length in rats with injury and stimulation was 163,401 ± 52,932μm, and length in rats with injury only was 71,947 ± 13,060μm; this change was not significant (P=0.06).

Comparing the effect size of stimulation on the two halves of the spinal cord, there was 2 times greater outgrowth to impaired side (ipsilateral) compared to the unimpaired (contralateral). In rats with injury only, axon length was 39.3 ± 4.7 times greater in the contralateral spinal cord compared to the ipsilateral spinal cord (i.e., ratio of total contralateral axon length/total ipsilateral axon length). In rats with injury and stimulation, the ratio dropped to 21.4 ± 7.0 (P=0.008, t-test of ratios). This demonstrates that stimulation increased axon length more on the sparsely innervated ipsilateral side compared with the dense contralateral side. When considering individual animal data, it is important to note that variability in axon length (Fig. 5C) was much larger for the injury and stimulated rats than injury alone. Since variability was small in the injury only group, indicating that our measurement techniques were highly consistent from animal to animal, a possible source of variability among the injury and stimulated rats was different responses to treatment.

Outgrowth directed preferentially to sparsely innervated regions of the spinal cord

We next mapped local axon length to determine the regional distribution changes in the contralateral and ipsilateral gray matter induced by electrical stimulation. In rats with or without stimulation, CST terminations are dense contralateral and sparse ipsilateral to the M1 of origin. To examine changes in the distribution of CST axons on the ipsilateral and

contralateral sides produced by stimulation, we expressed local axon length across all the animals as color-coded maps in Figure 6. To minimize the effect of differences in the size and shape of the C6 spinal cord across animals, we warped the gray matter of individual animals into a standard form. Stereological estimates of axon length were used to create local axon length. Note, the axon length scales are different on the two sides to show the full range on each side.

The group data show remarkable differences in intensity and distribution between the two halves of the spinal cord and between rats receiving injury only (Fig. 6A) and those that received stimulation after injury (Fig. 6B). The regional distributions of the ipsilateral (Fig. 6A, left) and contralateral (Fig. 6A, left) terminations are different in rats with injury only: the ipsilateral terminations are densest medially in the intermediate zone while contralateral terminations are densest in the deep dorsal horn. This differential termination pattern in the two halves of the spinal cord was also present in uninjured animals using a similar protocol for BDA labeling of M1 (Brus-Ramer et al., 2007), indicating that it is not due to injury-related CST outgrowth. The regional density of axons is markedly higher bilaterally in rats with stimulation (6B) after injury compared to those with injury only (6A), and the relative distribution is altered as well. On the ipsilateral side (6B, left), the axon density is greatest in the normally dense medial aspect of the intermediate zone. However, there is another dense area dorsal to the distribution seen in rats with injury only. On the contralateral side (6B, right), the densest area of BDA axons extends more dorsally than in rats with injury only.

We next determined where within the contralateral and ipsilateral spinal gray matter the stimulation-induced outgrowth occurred. For each location in the gray matter, we divided the pixel value of CST axon density for rats with injury and stimulation by the pixel value for rats with injury alone. This generated a color-coded regional distribution map of the ratio of the effect of injury and stimulation to injury alone (Fig. 6C). The larger the ratio, the proportionately greater effect that stimulation had at that site. We tested the hypothesis that increases in axon length contralaterally would be directed outside the densest area of innervation, likely because of competition within the stimulated system. The stimulation-induced outgrowth contralateral to stimulation (Fig. 6C, right) was greatest within laminae 3 and 4. There is additional outgrowth in the intermediate zone, and within lamina 9.

To further elucidate where stimulation increased CST axon length, we plotted total axon length at each dorsoventral gray matter depth. This is shown in Figure 6D. The blue line represents rats with injury only (corresponds to Fig. 6A), the red line represents rats with injury and stimulation (corresponds to Fig. 6B), and the black line represents the ratio (corresponds to Fig. 6C). Like the regional axon length maps, these have been scaled to show ipsilateral and contralateral outgrowth relative to one another (note differences in scales at bottom). The total axon length within each half of the spinal cord (Fig. 5C) is proportional to the area under the curve for the red and blue lines. For rats with injury only, the peak density along the dorsoventral axis for the dense contralateral terminations is within the deep dorsal horn (blue arrow). With stimulation, the distribution shifts dorsally (red arrow).

What is particularly striking on the contralateral side is that stimulation-induced outgrowth (black line and arrows on right; corresponds to right side of 5E) is directed outside the normal dense territory of the rats with injury only. Indeed, the dorsoventral distribution of stimulation-induced ratio of axon lengths represented by the black line is nearly the inverse of the axon density plot in the deep dorsal horn represented by the blue line. Thus, stimulation-induced an increase in axon length that is directed outside the densest CST territory. This finding fits with our prediction that stimulation directs local axon sprouting

preferentially within lower density areas and supports our hypothesis that competition within the stimulated system is a possible determinant of local outgrowth.

On the side ipsilateral to stimulation, we predicted that stimulation-induced increase in axon length would be greatest within the gray matter that had lost the dense innervation of the crossed CST. The dense contralateral projection after injury alone is densest within the medial aspect of the deep dorsal horn (Fig. 6A, right). This distribution is similar to the contralateral termination pattern in uninjured rats (Brus-Ramer et al, 2007). After pyramidotomy, there is loss of this dense contralateral projection from the hemisphere on the side of pyramidotomy. Stimulation after injury drives outgrowth preferentially to the territory that has lost the normal dense contralateral projection. This territory is outside of the typical ipsilateral distribution, which is located ventromedially (Brus-Ramer et al, 2007; Fig. 6A, left). Indeed, the densest area of stimulation-induced outgrowth on the ipsilateral side (Fig. 6C, left, black arrowhead) resembles the crossed projection (6A, right), with high density in the deep dorsal horn. In addition, stimulation-induced outgrowth extends ventrally, outside the region of greatest CST loss. We hypothesize that loss of competition from the dense contralateral projections of other half of the CST (competition between the two halves) is important for determining the pattern of ipsilateral outgrowth. This finding also raises the possibility that stimulation may restore similar CST circuits to the ones lost by injury, albeit at lower density.

The dorsoventral plot further elucidates the dorsal shift in axon density ipsilateral to M1 stimulation (Fig. 6D; left). The peak axon density for rats with injury alone (blue arrowhead) is within the intermediate zone. With stimulation, axon density still peaks in the intermediate zone (red arrowhead). However, the peak density of stimulation-induced outgrowth (black arrowhead) is within the deep dorsal horn. This suggests that the outgrowth due to stimulation is preferentially directed within the region of the normal dense crossed CST terminations from the other hemisphere. We propose that M1 stimulation partially restores the contralateral topography of CST terminations on the impaired ipsilateral side.

M1 stimulation promotes robust increase in corticofugal axon length in brain stem targets whether or not they are denervated by injury

Next, we asked whether M1 stimulation promotes a similar degree of increase in axon length in other subcortical targets important for forelimb function, the cuneate nucleus and the red nucleus. The cuneate nucleus relays touch and proprioception from the forelimb, and the red nucleus participates in limb motor control. The red nucleus is not denervated by pyramidotomy, while the cuneate is (Fig. 1A, as confirmed histologically in a control animal; data not shown). This comparison, therefore, helps to determine a rule of stimulation-induced sprouting, if the magnitude and topography of axon length change are determined by the amount of denervation, e.g. loss of projections from M1 on the side of pyramidotomy. Our stereological methods allow us to directly compare axon length within each of these structures.

Cuneate nucleus

Unlike the red nuclei, which are rostral to pyramidotomy, the cuneate nuclei lose all their cortical innervation from M1 on the side of pyramidotomy (Fig. 7A). Thus, the cuneate innervation is similar to the spinal cord, and specifically the CST innervation of mechanosensory laminae (Molander et al., 1989). Innervation of the cuneate nucleus is dense contralateral to the M1 of origin and sparse ipsilateral (Lue et al., 1997; Fig. 7B). The stimulated M1 projects strongly to the contralateral cuneate nucleus, the side receiving mechanoreceptive input from the contralateral limb (7A, thickest black line). Thus, the same

M1 that controls movement through the crossed CST receives sensory information from that side of the body (Fig. 7A, gray lines).

Photomicrographs of BDA-labeled axons in the cuneate nuclei demonstrate sparse innervation ipsilaterally and denser innervation contralaterally. Each was greater in rats with injury and stimulation (6B2) compared with rats with injury only (6B1). The corrected axon length of M1 terminations in the cuneate nuclei is presented in Figure 7C. Ipsilateral to M1 stimulation, the axon length was 2.1 times greater in rats with stimulation after injury (3,315 ± 459μm) compared with injury only rats (1,615 ± 634μm), but this was not significant (P=0.053). Stimulation-induced increase in axon length was robust in the contralateral cuneate nucleus; axon length was 2.5 times greater in rats with injury and stimulation (57,786 ± 9,377μm) compared to rats with injury alone (23,334 ± 2,610μm; t-test P=0.006; corrected for multiple comparisons, P=0.012). Thus, unlike the spinal cord, increase in axon length in the densely innervated cuneate nucleus was significant, while outgrowth to the sparsely innervated one was not.

We also mapped local cortico-cuneate termination length using maps similar to the spinal cord (Fig. 7D). Axons are most dense in the ventral aspect of the nucleus, in the rats with injury alone (7D1). In rats with injury and stimulation (7D2), terminations are both denser and more widely distributed; the area of densest innervation has expanded dorsally. The map of stimulation-induced changes in axon length (7D3) shows greatest increases outside the region of densest innervation in the rats with injury only, for both the contralateral and ipsilateral cuneate nuclei. Thus, M1 electrical stimulation promotes increase in axon length that is greatest outside the region of densest cortical projections. This suggests competition within the stimulated system is an important determinant of local sprouting. However, the total stimulation-induced increase in axon length was greater in the dense contralateral projection than the sparse ipsilateral side, indicating that in the cuneate nucleus, competition within the stimulated M1 terminations reflects may affect local, but not total, increase in axon length.

Parvocellular red nucleus

We examined the two functional divisions of the red nucleus, the parvocellular and the magnocellular. Both divisions receive a dense ipsilateral and sparse contralateral projections from M1 (Z'Graggen et al.; 2000, Brown, 1974;), and this pattern was observed after pyramidotomy (Fig. 8B). The parvocellular red nucleus receives a denser projection than the magnocellular division(Brown, 1974; Z'Graggen et al., 2000; 8B). The parvocellular red nucleus is part of a double-crossed olivocerebellar loop (Fig. 8A); it does not have a major spinal cord projection (Flumerfelt, 1978). Since CST connections are largely crossed, the net effect of the parvocellular red nucleus is to control contralateral limb movement.

Similar to the spinal cord and cuneate nucleus, we compared parvocellular red nucleus axon length in rats with injury and stimulation to rats with injury only. Figure 8C shows normalized axon length for the ipsilateral and contralateral parvocellular red nucleus. Ipsilateral to M1, labeled CST axon length was 2.1 times greater in rats with injury and stimulation (222,316 ± 84531μm) than rats with injury only (87,023 ± 14,316μm; t-test P=0.004; corrected for multiple comparisons, p=0.012). On the more sparsely innervated contralateral side, axon length was 2.3 times higher in rats with injury and stimulation (22,734 ± 9,752μm) compared with rat with injury only (7,156 ± 2,374μm), however this was not significantly different (P=0.09). Thus, like the cuneate nucleus, only the dense M1 projection was significantly increased by stimulation.

Like the other targets of M1, we mapped the distribution of parvocellular red nucleus terminations. Figure 8D presents local axon length maps, all scaled to display the full range

of values. In rats with injury only (8D1), the densest terminations in the two red nuclei largely do not overlap, which is similar to the spinal cord. For rats with injury and stimulation (8D2), there was also a difference in the regions of parvocellular red nucleus innervated by the ipsilateral and contralateral projections. Thus, the fact that the densest M1 projections to the parvocellular red nucleus target different regions in rats with injury only is similar to the spinal cord and implies competition between the corticorubral connections from each M1 at baseline. However, the fact that axon length changed only in the dense projection is similar to the cuneate nucleus, indicating that overall outgrowth may not be affected by competition within the stimulated terminations.

We also mapped local changes in axon length with stimulation (8D3) in the parvocellular red nucleus by creating a ratio of local axon length before and after stimulation. For both the contralateral and ipsilateral sides, increased axon length was found largely outside of the distribution of dense axons in rats with injury only. This effect was more obvious for the ipsilateral side. Thus, stimulation-induced changes in axon length appear to obey similar rules for within system competition as the spinal cord and cuneate nucleus, even if these effects are not as sharply demarcated as in the spinal cord.

Magnocellular red nucleus

As shown in Figure 9, we also measured the length of the M1 terminations in the magnocellular red nucleus. Like the parvocellular red nucleus, projections to the magnocellular portion are dense ipsilateral to M1 and sparse contralateral (9B). The sparse connections to the contralateral red nucleus could provide motor control signals through the rubrospinal tract from that red nucleus to the impaired side of the spinal cord (Fig. 9A, red, a double-crossed connection). Stimulation increased axon length in the magnocellular portion of both red nuclei (9B2 compared to 9B1). Axon length estimates are presented in Figure 9C. Ipsilateral to stimulation, axon length was 5.6 times greater in rats with injury and stimulation (47,525 ± 9,126μm) than in rats with injury only (8,547 ± 4,077μm; t-test P=0.006; corrected for multiple comparisons, p=0.012). Contralateral to stimulation, labeled CST axon length was 3.3 times greater in rats with injury and stimulation (4,126 ± 532μm) compared with injury-only rats (1,269 ± 529μm; t-test p=0.005; corrected for multiple comparisons, P=0.012). Unlike the spinal cord, the effect of stimulation was not different between the ipsilateral and contralateral magnocellular red nuclei (t-test ratios P=0.48). Thus, stimulation drives increases in axon length in the magnocellular portion of the red nucleus bilaterally.

Like the other M1 targets we analyzed, we mapped the spatial distribution of axon length within the magnocellular red nucleus for rats with injury only (Fig. 9D1) and rats with injury and stimulation (Fig. 9D2). In both groups, forelimb corticorubral connections targeted the forelimb area of the red nucleus, located in the medial and dorsal aspect of the nucleus (Murray & Gurule, 1979; Strominger *et al.*, 1987), on both ipsilateral and contralateral sides. For both groups of rats, but particularly for the rats with injury only, the pattern of innervation was more similar for the two sides (like the cuneate nucleus) than different (like the parvocellular red nucleus and spinal cord). This suggests that competition between projections from each M1 may not be a large determinant of the topographical distribution at baseline.

In keeping with the analysis of axon outgrowth in other regions, we mapped stimulation-induced change in axon length (Fig. 9D3). For the ipsilateral side, increase in axon length (9D3, left) was greatest outside of the distribution of dense corticofugal axons in rats with injury only (9D1, left). By contrast, on the contralateral side axon length increased most (9D3, right) within the densest region of rats with injury only (Fig. 9D1, right). Similar to the spinal cord, axon growth on the side that could most likely restore function fell within

the distribution of the normally dense projection from M1 on the side of pyramidotomy. In addition, the difference in outgrowth to the magnocellular red nuclei suggests two complementary set of rules, one driven by competition within the stimulated system in the red nucleus controlling the unaffected limb and a second set of rules for the red nucleus controlling the affected limb.

Origin of increased axon terminations

To investigate the path by which M1 axons reach their target, we use a traditional measure of axonal plasticity, the number of axons crossing midline. We measured the number of midline axons in the spinal cord and red nucleus, where corticofugal axons cross at the level of target innervation. In the spinal cord, contralateral axons cross the midline (i.e., recross) at the segmental level (Brosamle & Schwab, 1997; Brus-Ramer *et al.*, 2007; Rosenzweig *et al.*, 2009). To estimate change in the number of recrossing axons due to stimulation, we counted the number of axons between the midline of the gray matter and a line 25μm lateral to midline on the ipsilateral side. In rats with injury only, the average number of axons per 40μm section was 2.3 ± 0.5, and the number in rats with injury and stimulation was 4.8 ± 1.5. Although the effect size was large in the present study (2.2 times more axons with stimulation), this did not reach significance (P=0.07). We previously reported a similar, but significant, increase (1.7 times) in midline crossing CST axons in rats with pyramidotomy and stimulation killed right after the 10-day stimulation period, as opposed to 32–33 days after stimulation in the present study. This suggests that an increase in recrossing CST axons contributes only a portion of the increase in ipsilateral CST axon length.

Similar to the spinal cord, we counted the number of axons at the midline between the red nuclei as a possible marker of activity-dependent outgrowth. We examined the area between midline and a line 25μm lateral towards the contralateral red nucleus with the dorsoventral limits set by the red nuclei boundaries. Note, midline axons in the midbrain pass through bands of white matter (Paxinos & Watson, 1986), while recrossing axons in the spinal cord pass through gray matter (Figs. 5B). We examined all of the sections used to count axon length in both the parvocellular and magnocellular portions of red nucleus. The number of crossing axons between the parvocellular red nuclei for rats with injury and stimulation (29.7 ± 2.1) was not different than rats with injury only (37.5 ± 7.8; P=0.36). Between the magnocellular red nuclei, the number of crossing axons was lower than the parvocellular, and was also was not different in rats with injury and stimulation (10.8 ± 2.4) compared with rats with injury alone (18.2 ± 2.3; P=0.06). Although stimulation did not have an effect on crossing axons in both the spinal cord and red nucleus, there was strong trend towards increased number of crossing axons in the spinal cord, while no such trend was evident in the red nucleus. Thus, stimulation drove increases in axon termination length to the red nuclei, but not through the white matter between the red nuclei.

DISCUSSION

Axon outgrowth likely parallels the functional connectivity underlying motor recovery (Carmel et al., 2010), so we determined how electrical stimulation of M1 after pyramidotomy sculpts spared connections. We identify four main findings. First, stimulation produces a 2- to 5-fold, increase in corticofugal axon terminations in red nucleus, cuneate nucleus, and spinal cord. Second, stimulation-induced axon outgrowth was similarly robust in the red nucleus, which was not denervated, as structures that were denervated by pyramidotomy, the spinal cord and cuneate nucleus, suggesting that stimulation-induced outgrowth does not depend strongly on loss of innervation from the other M1. Third, analysis of the regional distribution of corticofugal label showed that axon outgrowth from the stimulated M1 was preferentially directed outside the areas that normally have the highest corticofugal innervation, suggesting strong local competition within the stimulated

system. Finally, stimulation drove outgrowth to circuits normally controlling the impaired forelimb, suggesting that adaptive circuits were reformed by stimulation. This topographical shift was strongest in the ipsilateral spinal cord but was also present in the magnocellular red nucleus. Our findings suggest that M1 stimulation does not simply produce a global increase in corticospinal system connectivity because the increased corticofugal terminations showed topographic specificity.

Stimulation drives robust outgrowth to structures controlling the impaired forelimb

Unilateral pyramidotomy in rats produces contralateral deficits in skilled limb control (Whishaw & Metz, 2002; Carmel *et al.*, 2010). Chronic stimulation of forelimb M1 on the intact side fully restores skilled forelimb motor function (Carmel et al., 2010) and increases CST termination density and strength on the impaired side of the spinal cord (Brus-Ramer et al., 2007; Carmel et al., 2010), ipsilateral to stimulation. In the present study we found that, in addition to ipsilateral spinal connections, M1 connections to brain stem nuclei that are important in limb control also were enhanced. This too may improve motor control in the impaired forelimb. The rubrospinal and corticospinal systems have overlapping functions, particularly in distal limb control (Martin & Ghez, 1988; Cheney *et al.*, 1991). In the cuneate nucleus, M1 projections can modify proprioceptive information from large diameter sensory fibers (Andersen *et al.*, 1962; Ghez & Pisa, 1972). Strengthening the connections between stimulated M1 and the ipsilateral cuneate nucleus could improve skilled motor control (Ghez & Sainburg, 1995) by modulating afferent information from the affected forelimb. In addition, there are other corticofugal targets that could participate in recovery of function, including reticulospinal tract neurons. The indirect cortico-reticular projection has been shown to be an important pathway for activation of spinal motoneurons (Jankowska & Edgley, 2006). These findings suggest that the motor recovery produced by stimulation may occur through both direct spinal and indirect brain stem connections to spinal motor circuits, as well as through novel somatic sensory regulation.

Stimulation induces outgrowth to M1 targets whether or not they are denervated by pyramidotomy

Activity-dependent competition between CST spinal terminations from each hemisphere determines their proper topography during development (Martin et al., 2007). We determined the rules of these interactions using a combination of neural inactivation, limb constraint, and electrical stimulation first to disturb normal development, and later to restore proper connections (Martin et al., 2009). As we harness activity to repair the injured adult corticospinal system (Brus-Ramer et al., 2007), we also attempt to understand how exogenous activity helps direct new circuit formation.

We found different effects of stimulation in the spinal cord and the brain stem. While, as a percentage, the outgrowth to the spinal cord was preferentially directed to the sparse, impaired side, relative outgrowth was similar to the sparsely- and densely-innervated sides of the red nucleus and the cuneate nucleus. Since this is not explained by a denervation affect, one possible reason for this is that the sources of competition for the stimulated axons differ between targets. In the ipsilateral spinal cord, the greatest source of competition is likely the crossed CST from the other hemisphere, as supported by our developmental findings (Martin *et al.*, 1999; Martin & Lee, 1999) and the difference in topography at baseline. We propose that release of this competition after pyramidotomy is what causes sprouting of ipsilateral connections(Brus-Ramer et al., 2007). Stimulation after pyramidotomy also drives greater outgrowth on this side because there is little competition between each of the stimulated terminations (i.e., because they are sparse). In contrast, the stimulated terminations on the contralateral, unimpaired, side of the spinal cord are very dense and likely compete strongly with one another, limiting stimulation-induced axon

outgrowth. Possible mechanisms underlying these interactions are discussed below. At the red nucleus, pyramidotomy does not remove the corticorubral innervation from M1 on the lesioned side. On the side of the pyramidotomy, the red nucleus continues to receive a dense projection from M1 and sparse corticorubral terminations from the opposite, intact, side. We propose that the sparse corticorubral terminations that are stimulated compete with dense projections from M1 on the side of pyramidotomy, possibly limiting the magnitude of their outgrowth. Finally, the cuneate nucleus loses all innervation from M1 on the side of pyramidotomy. However, the strongest terminations in the cuneate nucleus are from large-diameter forelimb afferents, which are also likely the greatest source of competition to limit stimulation-induced CST outgrowth.

It is important to note that although stimulation produced outgrowth to circuits that were not denervated by pyramidotomy, this did not appear to have any deleterious effects. Rats behaved normally, and the motor performance of the unimpaired limb did not change throughout the stimulation and follow up period (30 days) (Carmel et al., 2010).

Competition within stimulated M1 terminations

Stimulation-induced outgrowth was preferentially directed outside the areas of highest corticofugal axon density in spinal cord and brain stem, suggesting activity-dependent competition between stimulated M1 terminations. Consistent with this, percent outgrowth in ipsilateral spinal cord, with normally sparse CST terminations, was greater than outgrowth contralaterally, where CST terminations are dense. By contrast, brain stem outgrowth appeared not to be limited by corticofugal termination density. However, in the spinal cord, where the total axon length contralateral to M1 was more than forty times greater than the length ipsilateral to M1, the outgrowth was greatest to the ipsilateral side. Thus, there may be a density threshold for within-system competition that limits growth into higher density regions and permits growth to very sparse areas. Indeed, there is evidence for density-dependent competition between axon terminations both in vitro (She & Craig, 2011) and in vivo (Hua et al., 2005).

Increases in axon length induced by electrical stimulation may involve stabilization of axon terminations, increased branching, or de novo outgrowth (Gibson & Ma, 2011). Several molecular mechanisms may explain the increased outgrowth with stimulation, including more efficient use of trophic factors, activity-regulated release of trophic factors, or direct regulation of growth intrinsically by activity. Activity, or simulation of activity with the cAMP agonist foskolin, can dramatically increase axon outgrowth in response to trophic factors (Goldberg *et al.*, 2002a). Increased outgrowth results from a convergence of intracellular signaling between neurotrophins and activity, which are synergistic (Singh & Miller, 2005). In addition, activity causes release of neurotrophins, including BDNF (Kuczewski et al., 2009), which promotes sprouting of corticospinal axons (Ozdinler & Macklis, 2006). Finally, activity can boost the intrinsic growth state of axons (Goldberg *et al.*, 2002b; Van Ooyen, 2005). Exploration of cellular mechanisms of stimulation-induced outgrowth will be critical for understanding the relationship of this potential therapy to other therapies that target spared connections after injury (Raineteau & Schwab, 2001; Hagg, 2006).

Reforming lost connections

After focal central nervous system damage, alternate circuits can restore function by rerouting signals from above to below the injury. These circuits can arise spontaneously (Bareyre *et al.*, 2004; Courtine *et al.*, 2008) or they can be engineered to bypass the injury (Campos *et al.*, 2004; Campos *et al.*, 2008; Tom *et al.*, 2009; Alilain *et al.*, 2011). An outstanding question is how much these new circuits must resemble the injured ones to

restore function. In the spinal cord, the pattern of local axon density on the impaired side changed markedly with stimulation. Stimulation-induced outgrowth was greatest in the deep dorsal horn, similar to the normal crossed CST distribution (Curfs *et al.*, 1994; Brus-Ramer *et al.*, 2007). This suggests that electrical stimulation drove spinal axon termination outgrowth into a pattern resembling the one that normally controls skilled forelimb movement contralaterally. Similarly, in the magnocellular red nucleus, stimulation drove contralateral outgrowth to the dorsomedial red nucleus, which represents the forelimb. This suggests a preferential targeting of circuits that could restore forelimb function, such as ipsilateral CST connections with key spinal interneurons or contralateral corticorubral connections with rubrospinal neurons.

The targeting of adaptive circuits does not depend on denervation of the target, since a similar effect was seen in the denervated spinal cord as was seen in the non-denervated magnocellular red nucleus. It is also interesting to note that the circuits showing the targeting effect have the most direct access to the impaired side of the spinal cord. The differential contributions of the direct projection of M1 to the impaired side of the spinal cord and the cortico-rubro-spinal circuit to recovery of motor skills will be an important issue for future study. This investigation will help us understand how stimulation should be applied to regain control of spinal circuits. In turn, this will inform translational efforts using electrical stimulation to strengthen residual circuits after brain and spinal cord injury.

Acknowledgments

We thank Drs. Martina Pavlicova and Jessica Elder for their assistance with statistical analyses, Xiuli Wu for histochemistry and histology, and Dr. Kathleen Friel for help with MATLAB. This work was supported by National Institutes of Health grants TL1RR024158 (J.B.C.) and R01NS64004 (J.H.M.) and a Christopher and Dana Reeve Foundation grant (J.B.C).

ABBREVIATIONS

BDA	biotinylated dextran amine
CST	corticospinal tract
M1	primary motor cortex
GFAP	glial fibrillary acidic protein.

REFERENCES

Alilain WJ, Horn KP, Hu H, Dick TE, Silver J. Functional regeneration of respiratory pathways after spinal cord injury. Nature. 2011; 475:196–200. [PubMed: 21753849]

Andersen P, Eccles JC, Schmidt RF. Presynaptic inhibition in the cuneate nucleus. Nature. 1962; 194:741–743. [PubMed: 13861183]

Bareyre FM, Kerschensteiner M, Raineteau O, Mettenleiter TC, Weinmann O, Schwab ME. The injured spinal cord spontaneously forms a new intraspinal circuit in adult rats. Nat Neurosci. 2004; 7:269–277. [PubMed: 14966523]

Brosamle C, Schwab ME. Cells of origin, course, and termination patterns of the ventral, uncrossed component of the mature rat corticospinal tract. J Comp Neurol. 1997; 386:293–303. [PubMed: 9295153]

Brown LT. Rubrospinal projections in the rat. J Comp Neurol. 1974; 154:169–187. [PubMed: 4826093]

Brus-Ramer M, Carmel JB, Chakrabarty S, Martin JH. Electrical stimulation of spared corticospinal axons augments connections with ipsilateral spinal motor circuits after injury. J Neurosci. 2007; 27:13793–13801. [PubMed: 18077691]

Brus-Ramer M, Carmel JB, Martin JH. Motor cortex bilateral motor representation depends on subcortical and interhemispheric interactions. J Neurosci. 2009; 29:6196–6206. [PubMed: 19439597]

Campos L, Meng Z, Hu G, Chiu DT, Ambron RT, Martin JH. Engineering novel spinal circuits to promote recovery after spinal injury. J Neurosci. 2004; 24:2090–2101. [PubMed: 14999060]

Campos LW, Chakrabarty S, Haque R, Martin JH. Regenerating motor bridge axons refine connections and synapse on lumbar motoneurons to bypass chronic spinal cord injury. J Comp Neurol. 2008; 506:838–850. [PubMed: 18076081]

Carmel JB, Berrol LJ, Brus-Ramer M, Martin JH. Chronic electrical stimulation of the intact corticospinal system after unilateral injury restores skilled locomotor control and promotes spinal axon outgrowth. J Neurosci. 2010; 30:10918–10926. [PubMed: 20702720]

Cheney PD, Fetz EE, Mewes K. Neural mechanisms underlying corticospinal and rubrospinal control of limb movements. Prog Brain Res. 1991; 87:213–252. [PubMed: 1866448]

Courtine G, Song B, Roy RR, Zhong H, Herrmann JE, Ao Y, Qi J, Edgerton VR, Sofroniew MV. Recovery of supraspinal control of stepping via indirect propriospinal relay connections after spinal cord injury. Nat Med. 2008; 14:69–74. [PubMed: 18157143]

Curfs MH, Gribnau AA, Dederen PJ. Selective elimination of transient corticospinal projections in the rat cervical spinal cord gray matter. Brain Res Dev Brain Res. 1994; 78:182–190.

Faul F, Erdfelder E, Lang AG, Buchner A. G*Power 3: a flexible statistical power analysis program for the social, behavioral, and biomedical sciences. Behav Res Methods. 2007; 39:175–191. [PubMed: 17695343]

Flumerfelt BA. Organization of the mammalian red nucleus and its interconnections with the cerebellum. Experientia. 1978; 34:1178–1179. [PubMed: 102524]

Friel KM, Martin JH. Bilateral activity-dependent interactions in the developing corticospinal system. J Neurosci. 2007; 27:11083–11090. [PubMed: 17928450]

Ghez C, Pisa M. Inhibition of afferent transmission in cuneate nucleus during voluntary movement in the cat. Brain Res. 1972; 40:145–155. [PubMed: 4338259]

Ghez C, Sainburg R. Proprioceptive control of interjoint coordination. Can J Physiol Pharmacol. 1995; 73:273–284. [PubMed: 7621366]

Ghosh A, Sydekum E, Haiss F, Peduzzi S, Zorner B, Schneider R, Baltes C, Rudin M, Weber B, Schwab ME. Functional and anatomical reorganization of the sensory-motor cortex after incomplete spinal cord injury in adult rats. J Neurosci. 2009; 29:12210–12219. [PubMed: 19793979]

Gibson DA, Ma L. Developmental regulation of axon branching in the vertebrate nervous system. Development. 2011; 138:183–195. [PubMed: 21177340]

Goldberg JL, Espinosa JS, Xu Y, Davidson N, Kovacs GT, Barres BA. Retinal ganglion cells do not extend axons by default: promotion by neurotrophic signaling and electrical activity. Neuron. 2002a; 33:689–702. [PubMed: 11879647]

Goldberg JL, Klassen MP, Hua Y, Barres BA. Amacrine-signaled loss of intrinsic axon growth ability by retinal ganglion cells. Science. 2002b; 296:1860–1864. [PubMed: 12052959]

Hagg T. Collateral sprouting as a target for improved function after spinal cord injury. J Neurotrauma. 2006; 23:281–294. [PubMed: 16629616]

He Z. Fluorogold induces persistent neurological deficits and circling behavior in mice over-expressing human mutant tau. Curr Neurovasc Res. 2009; 6:54–61. [PubMed: 19355926]

Hua JY, Smear MC, Baier H, Smith SJ. Regulation of axon growth in vivo by activity-based competition. Nature. 2005; 434:1022–1026. [PubMed: 15846347]

Jankowska E, Edgley SA. How can corticospinal tract neurons contribute to ipsilateral movements? A question with implications for recovery of motor functions. Neuroscientist. 2006; 12:67–79. [PubMed: 16394194]

Kuczewski N, Porcher C, Lessmann V, Medina I, Gaiarsa JL. Activity-dependent dendritic release of BDNF and biological consequences. Mol Neurobiol. 2009; 39:37–49. [PubMed: 19156544]

Lue JH, Lai SM, Wang TJ, Shieh JY, Wen CY. Synaptic relationships between corticocuneate terminals and glycine-immunoreactive neurons in the rat cuneate nucleus. Brain Res. 1997; 771:167–171. [PubMed: 9383022]

Maier IC, Baumann K, Thallmair M, Weinmann O, Scholl J, Schwab ME. Constraint-induced movement therapy in the adult rat after unilateral corticospinal tract injury. J Neurosci. 2008; 28:9386–9403. [PubMed: 18799672]

Martin, J.; Friel, K.; Salimi, I.; Chakrabarty, S. Corticospinal Development. In: Squire, L., editor. Encyclopedia of Neuroscience. Oxford: Academic Press; 2009. p. 302-314.

Martin JH, Friel KM, Salimi I, Chakrabarty S. Activity- and use-dependent plasticity of the developing corticospinal system. Neurosci Biobehav Rev. 2007; 31:1125–1135. [PubMed: 17599407]

Martin JH, Ghez C. Red nucleus and motor cortex: parallel motor systems for the initiation and control of skilled movement. Behav Brain Res. 1988; 28:217–223. [PubMed: 3382515]

Martin JH, Kably B, Hacking A. Activity-dependent development of cortical axon terminations in the spinal cord and brain stem. Exp Brain Res. 1999; 125:184–199. [PubMed: 10204771]

Martin JH, Lee SJ. Activity-dependent competition between developing corticospinal terminations. Neuroreport. 1999; 10:2277–2282. [PubMed: 10439448]

Molander C, Xu Q, Rivero-Melian C, Grant G. Cytoarchitectonic organization of the spinal cord in the rat: II. The cervical and upper thoracic cord. J Comp Neurol. 1989; 289:375–385. [PubMed: 2808773]

Mouton PR, Gokhale AM, Ward NL, West MJ. Stereological length estimation using spherical probes. J Microsc. 2002; 206:54–64. [PubMed: 12000563]

Murray HM, Gurule ME. Origin of the rubrospinal tract of the rat. Neurosci Lett. 1979; 14:19–23. [PubMed: 530486]

Ozdinler PH, Macklis JD. IGF-I specifically enhances axon outgrowth of corticospinal motor neurons. Nat Neurosci. 2006; 9:1371–1381. [PubMed: 17057708]

Paxinos, G.; Watson, C. The Rat Brain in Stereotaxic Coordinates. Orlando: Academic Press, Inc; 1986.

Raineteau O, Schwab ME. Plasticity of motor systems after incomplete spinal cord injury. Nat Rev Neurosci. 2001; 2:263–273. [PubMed: 11283749]

Rosenzweig ES, Brock JH, Culbertson MD, Lu P, Moseanko R, Edgerton VR, Havton LA, Tuszynski MH. Extensive spinal decussation and bilateral termination of cervical corticospinal projections in rhesus monkeys. J Comp Neurol. 2009; 513:151–163. [PubMed: 19125408]

She K, Craig AM. NMDA Receptors Mediate Synaptic Competition in Culture. PLoS One. 2011; 6:e24423. [PubMed: 21935408]

Singh KK, Miller FD. Activity regulates positive and negative neurotrophin-derived signals to determine axon competition. Neuron. 2005; 45:837–845. [PubMed: 15797546]

Storey JD. A Direct Approach to False Discovery Rates. Journal of the Royal Statistical Society. Series B (Statistical Methodology). 2002; 64:20.

Strominger RN, McGiffen JE, Strominger NL. Morphometric and experimental studies of the red nucleus in the albino rat. Anat Rec. 1987; 219:420–428. [PubMed: 3448957]

Tom VJ, Sandrow-Feinberg HR, Miller K, Santi L, Connors T, Lemay MA, Houle JD. Combining peripheral nerve grafts and chondroitinase promotes functional axonal regeneration in the chronically injured spinal cord. J Neurosci. 2009; 29:14881–14890. [PubMed: 19940184]

Van Ooyen A. Competition in neurite outgrowth and the development of nerve connections. Prog Brain Res. 2005; 147:81–99. [PubMed: 15581699]

Watson, C.; Paxinos, G.; Kayalioglu, G. The Spinal Cord. London: Elsevier; 2009.

Whishaw IQ, Metz GA. Absence of impairments or recovery mediated by the uncrossed pyramidal tract in the rat versus enduring deficits produced by the crossed pyramidal tract. Behav Brain Res. 2002; 134:323–336. [PubMed: 12191820]

Z'Graggen WJ, Fouad K, Raineteau O, Metz GA, Schwab ME, Kartje GL. Compensatory sprouting and impulse rerouting after unilateral pyramidal tract lesion in neonatal rats. J Neurosci. 2000; 20:6561–6569. [PubMed: 10964961]

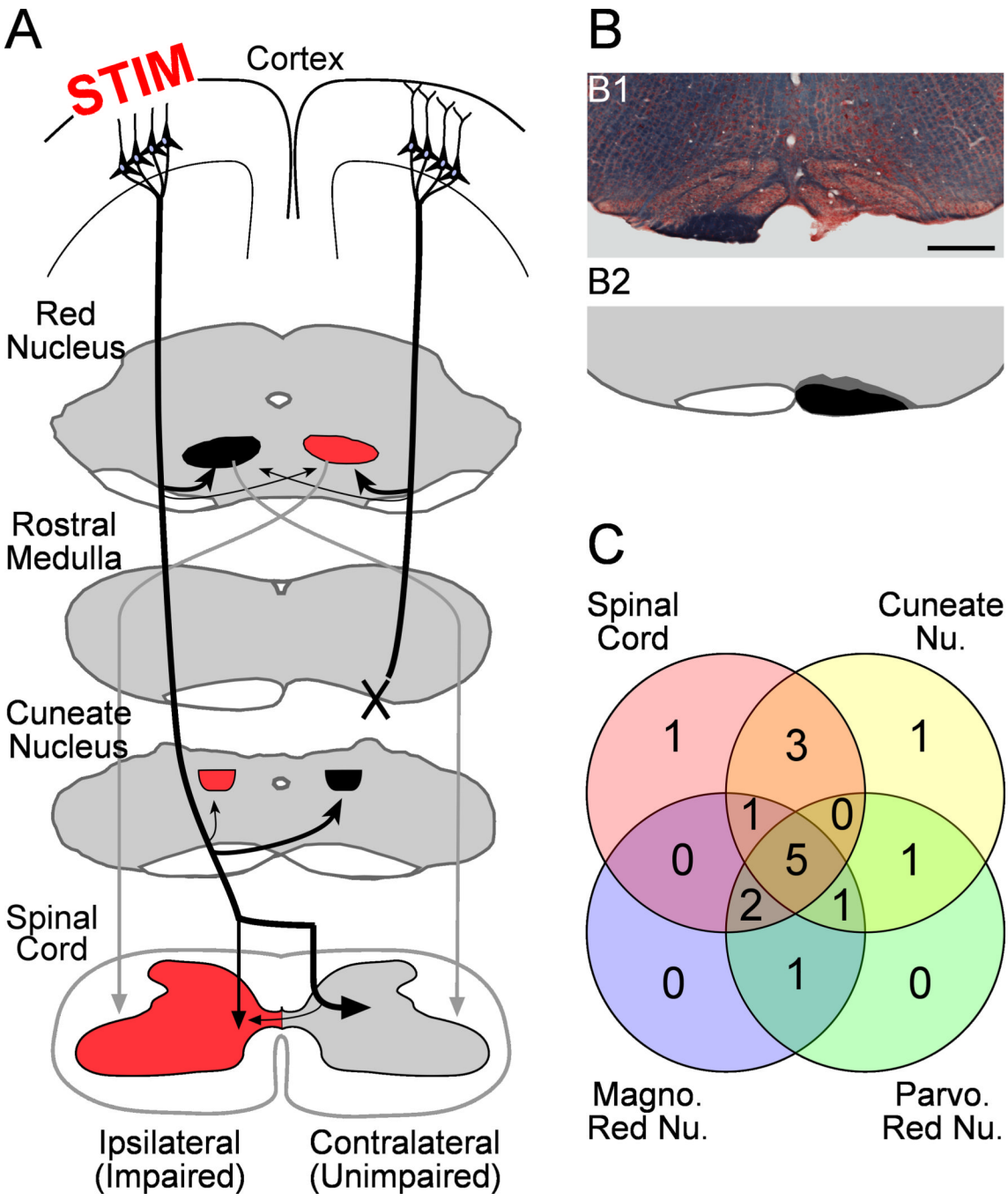

Figure 1.

A. Experimental schema. The CST from one hemisphere is cut (X; pyramidotomy) at the rostral medulla. This removes axon projections from M1 on the side of pyramidotomy to the spinal cord and cuneate nucleus but not the red nucleus. In the other hemisphere, an epidural electrode over forelimb M1 is used to deliver chronic electrical stimulation (STIM). The stimulated M1 is anterogradely labeled, and the corticofugal terminations measured in the spinal cord, cuneate nucleus, and red nucleus. Structures in red may be targeted to restore function of the impaired forelimb. B. Pyramidotomy completely severs the CST without extension into adjacent structures. B1. Kluver-Barera stain of the pyramidotomy site; the intact pyramid is dark blue. B2. The right pyramid shows a semi-schematic drawing of the

smallest (black) and largest (dark gray) lesions of the pyramid. C. The overlap of rats used for analysis of each M1 target.

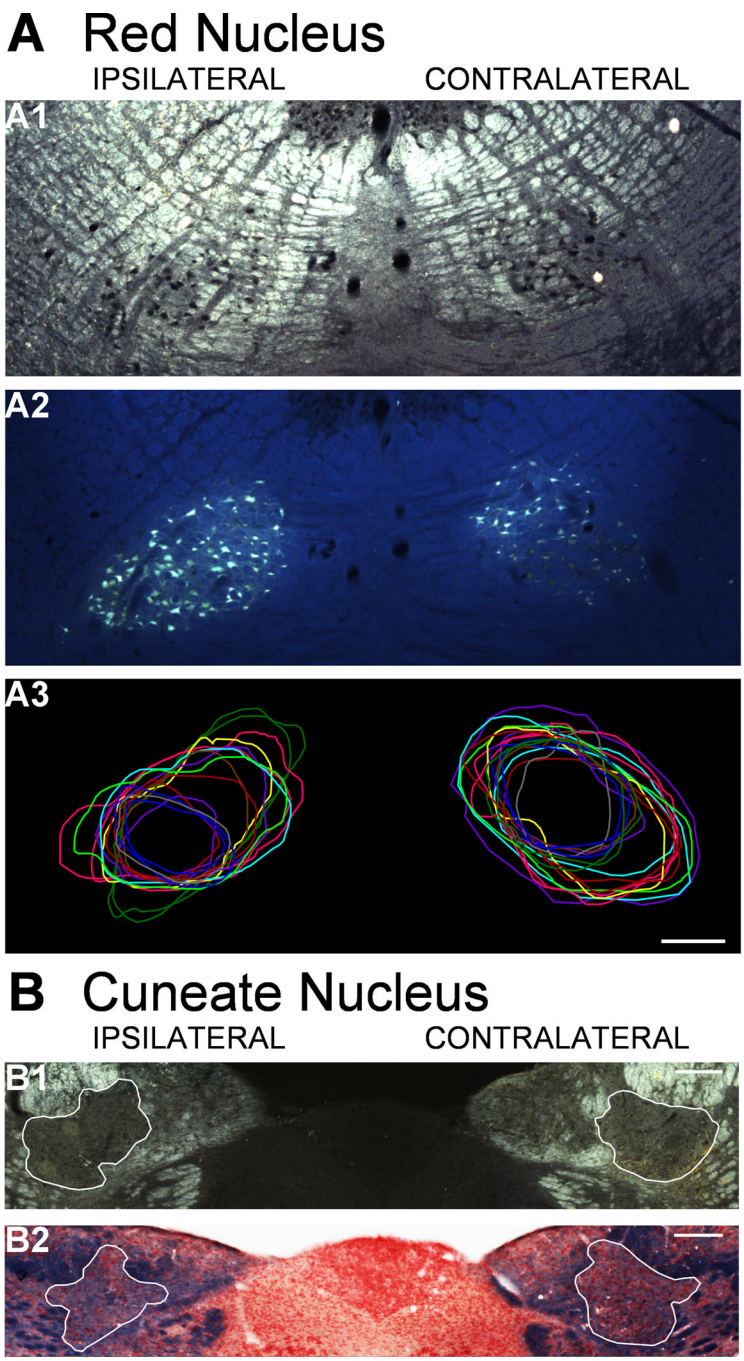

Figure 2.

Methods for defining the red nucleus and cuneate nucleus. A. Red nucleus. A1. Darkfield image of the red nuclei. The nuclear region was identified by the dark cell bodies. A2. Fluorescence image of the same section as A1. Fluorogold injected into C6 spinal gray matter labeled the magnocellular red nucleus. A3. Contours drawn under darkfield imaging to outline the parvocellular red nucleus in each animal (separate colors) were highly reproducible. Scale bar, 250μm. B. Cuneate nucleus. B1. Darkfield imaging of the caudal medulla is used to verify nucleus boundaries. B2. Kluver-Barrera staining of an adjacent section is used to validate the location for the nucleus (red) from the surrounding white matter (blue). Scale bars, 100μm.

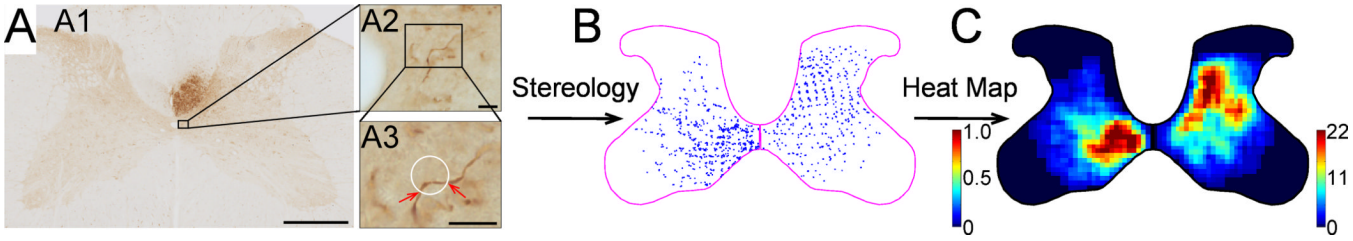

Figure 3.

Stereological methods of assessing axon length and regional distribution. A. BDA-labeled spinal cord cross section at C6. A1. Montage image of the gray matter. Scale bar, 500μm. A2. BDA-labeled axons at 400x. Scale bar, 10μm. A3. Axons intersect (red arrows) a virtual sphere ("space ball") that appears as a white circle of varying diameters. Scale bar, 10μm. B. A map of interactions between the "space ball" probe and BDA-labeled axons. The sparse ipsilateral side (left) was sampled more intensely than the dense contralateral side (right). C. Using MATLAB, heat maps of axon length within local regions (40μm by 40μm) are created. Note the difference in scaling of the two sides.

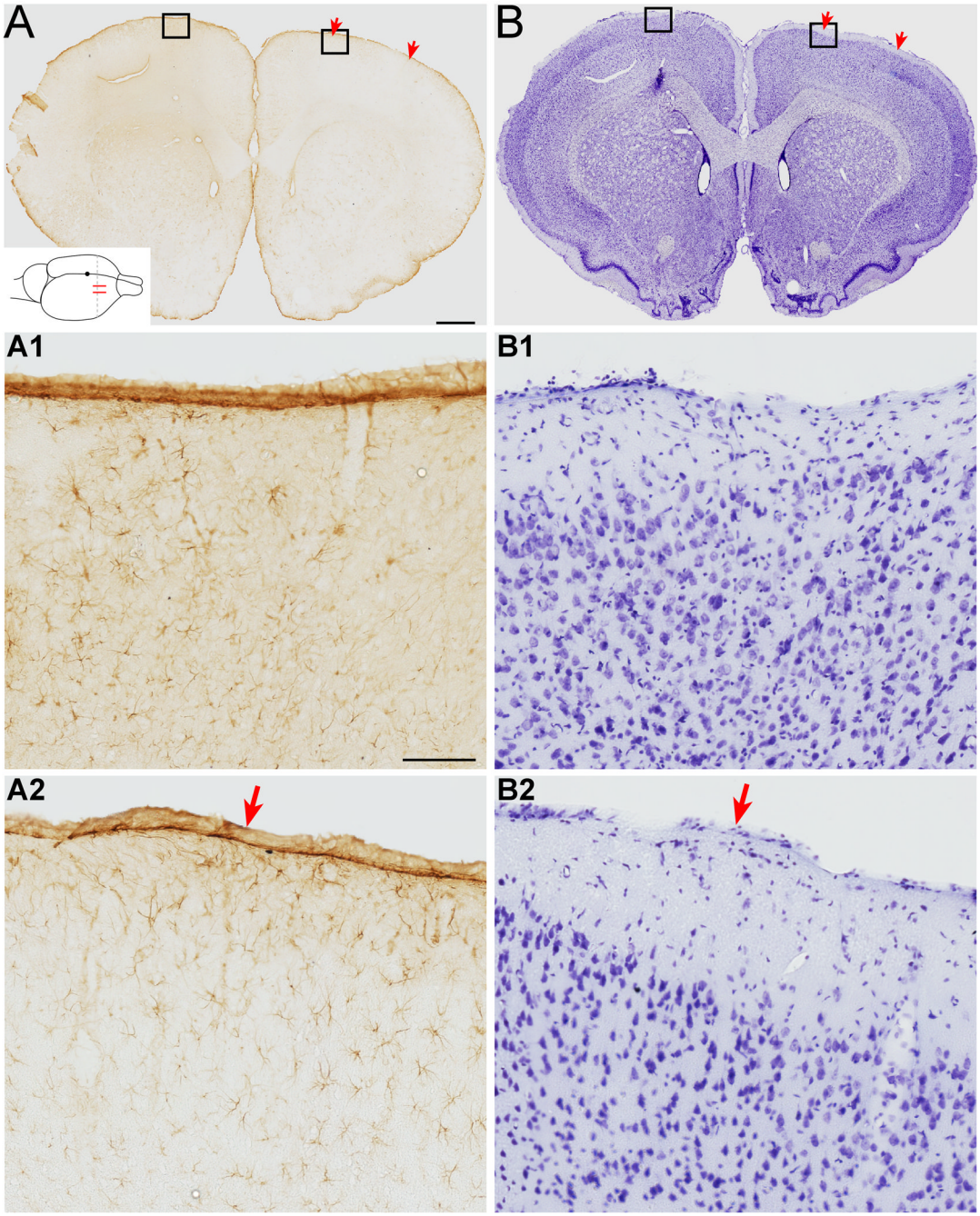

Figure 4.

Electrical stimulation does not produce gliosis or alter cellular architecture in M1. A. GFAP stained sections of cortex under the stimulating electrode section at approximately bregma +1.7mm from a rat with chronic epidural stimulation. The approximate position of the stimulating electrodes is marked with red arrows. Inset shows a schematic of stimulating electrodes (red) and plane of section for photomicrographs (interrupted line). The black dot represents bregma. There is no increase in overall GFAP signal in stimulated M1 compared with the non-stimulated side. Scale bar, 1mm. A1, A2 show high power images of M1. The glial cell architecture is similar for each. Scale bar, 100μm. B. Nissl stain of an adjacent section. The cellular architecture is similar for each motor cortex. B1, B2. Higher

magnification images of each M1 showing normal cellular morphology. Scale bars in A apply to B.

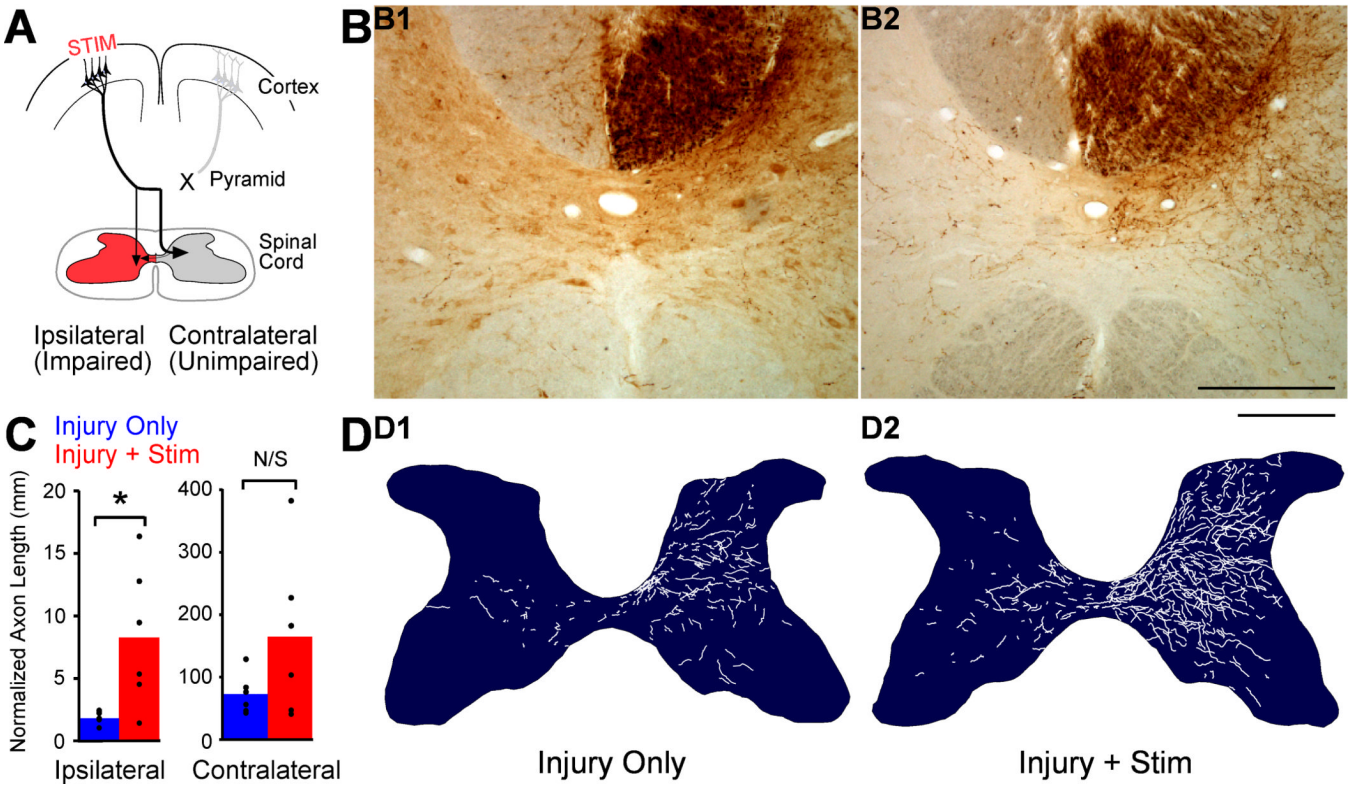

Figure 5.

M1 stimulation causes robust outgrowth to the spinal cord and targets the impaired side. A. Schema. Outgrowth to the impaired side of the spinal cord (red) is most likely to help restore function. B. BDA-labeled axons in C6 spinal cord cross section centered on the central canal. B1. A section from a representative injury only rat shows BDA-label is dense contralateral (right) and sparse ipsilateral (left). B2. A section from a representative injury and stimulation rat shows much greater axon label than in the rat with injury only. Scale bar, 250μm. C. Quantification of total axon length within each side of the spinal cord gray matter. D. Representative individual spinal cross-sections showing hand-traced BDA-labeled axons. D1 is traced from the section in B1, and D2 is traced from the section in B2.Scale bar, 500μm.

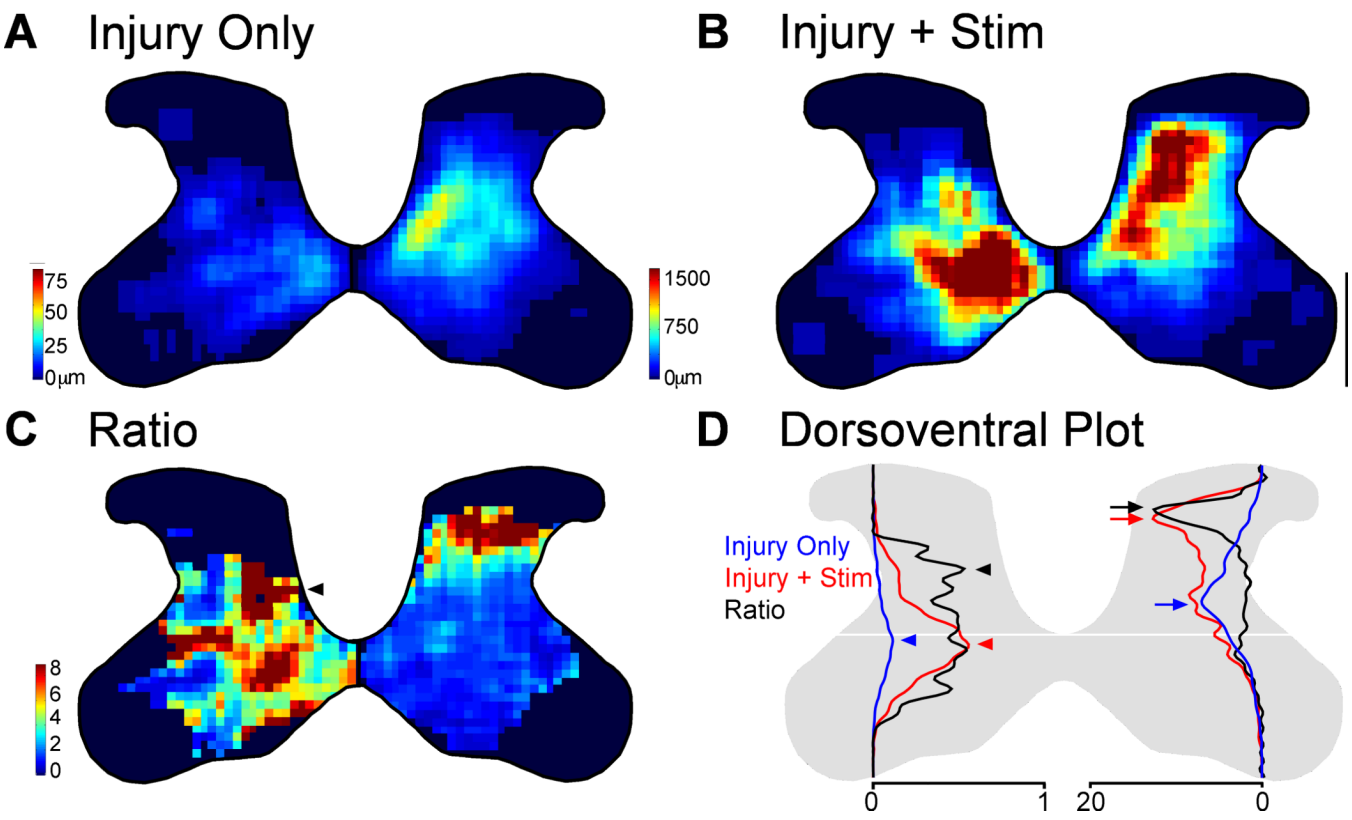

Figure 6.

Partial restoration of normal axon distribution on the impaired side of the spinal cord. A. Spatially corrected local axon length map for rats with injury only. B. Local axon length map for rats with injury and stimulation. Intensity scales in A also apply to B. Note, the axon length scales are different on the two sides to show the full range on each side. C. Stimulation-induced outgrowth is shown as the pixel-by-pixel ratio of injury and stimulation rats to injury only rats expressed as fold-change. The arrowhead indicates a hot spot of stimulation-induced outgrowth on the ipsilateral side in the deep dorsal horn. D. Dorsoventral distribution of axon density for rats with injury only (blue) and rats with injury and stimulation (red). The scales (bottom) on the two sides of the spinal cord are relative axon length apply only to the red and blue lines. Black lines represent the ratio of injury and stimulation rats to injury only rats and are scaled equivalently on the two sides. Arrows and arrowheads indicate peaks. Scale bar, 500μm. * $P<0.05$, corrected for multiple comparisons.

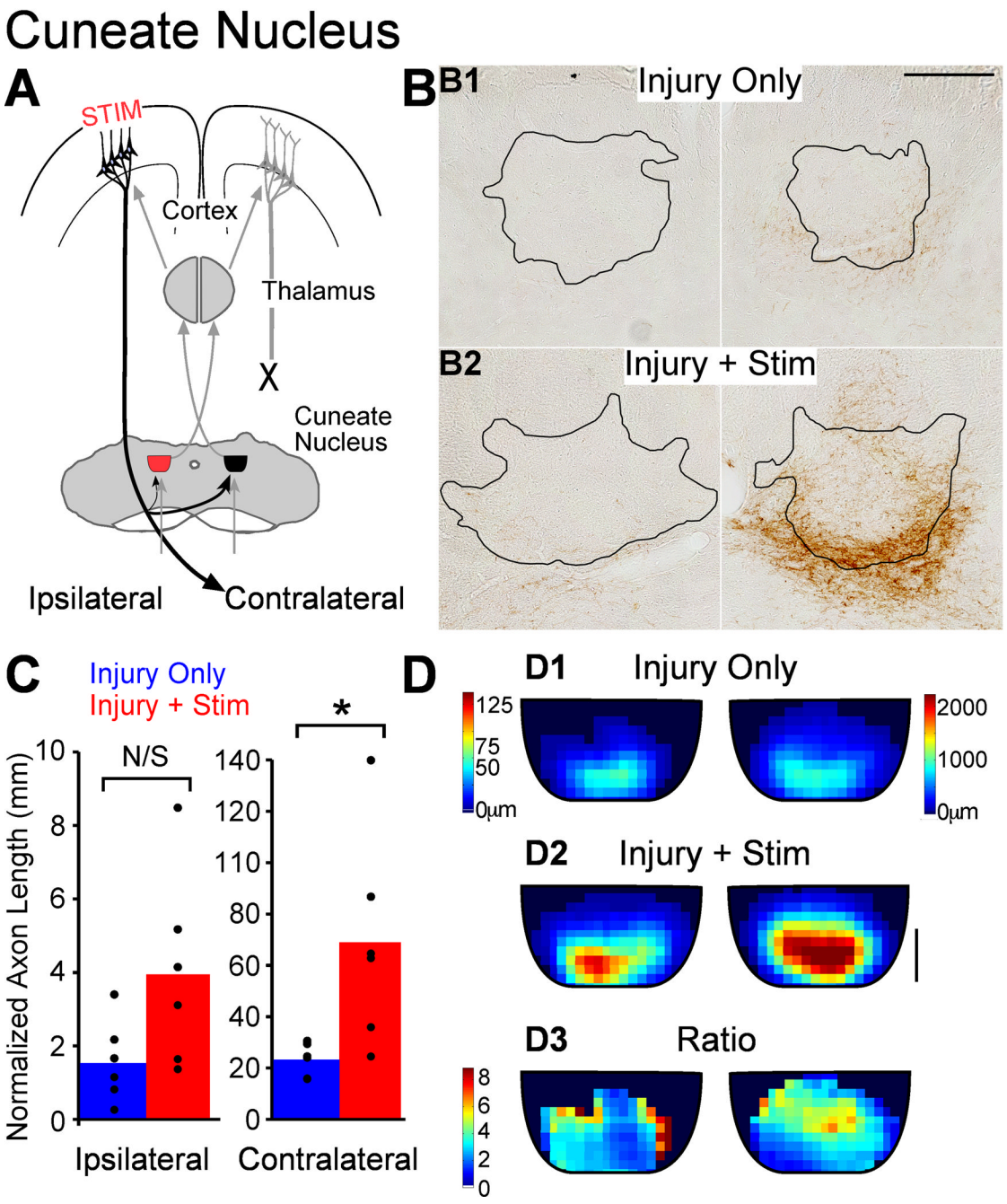

Figure 7.

M1 stimulation causes robust outgrowth to the cuneate nucleus. A. Schema. Outgrowth to the ipsilateral cuneate nucleus (red) could help modify sensory information projecting to M1 on the side of injury. B. Micrographs of BDA-labeled axons in cuneate nucleus (outlined) of representative rats. Scale bar, 250μm. C. Quantification of total axon length. D. Local axon length maps. Intensity scales in D1 also apply to D2. Note the axon length scales are different on the two sides to show the full range on each side. D3. Stimulation-induced outgrowth is shown as the pixel-by-pixel ratio of injury and stimulation rats to injury only rats expressed as fold-change. Scale bar, 100μm. * $P<0.05$, corrected for multiple comparisons.

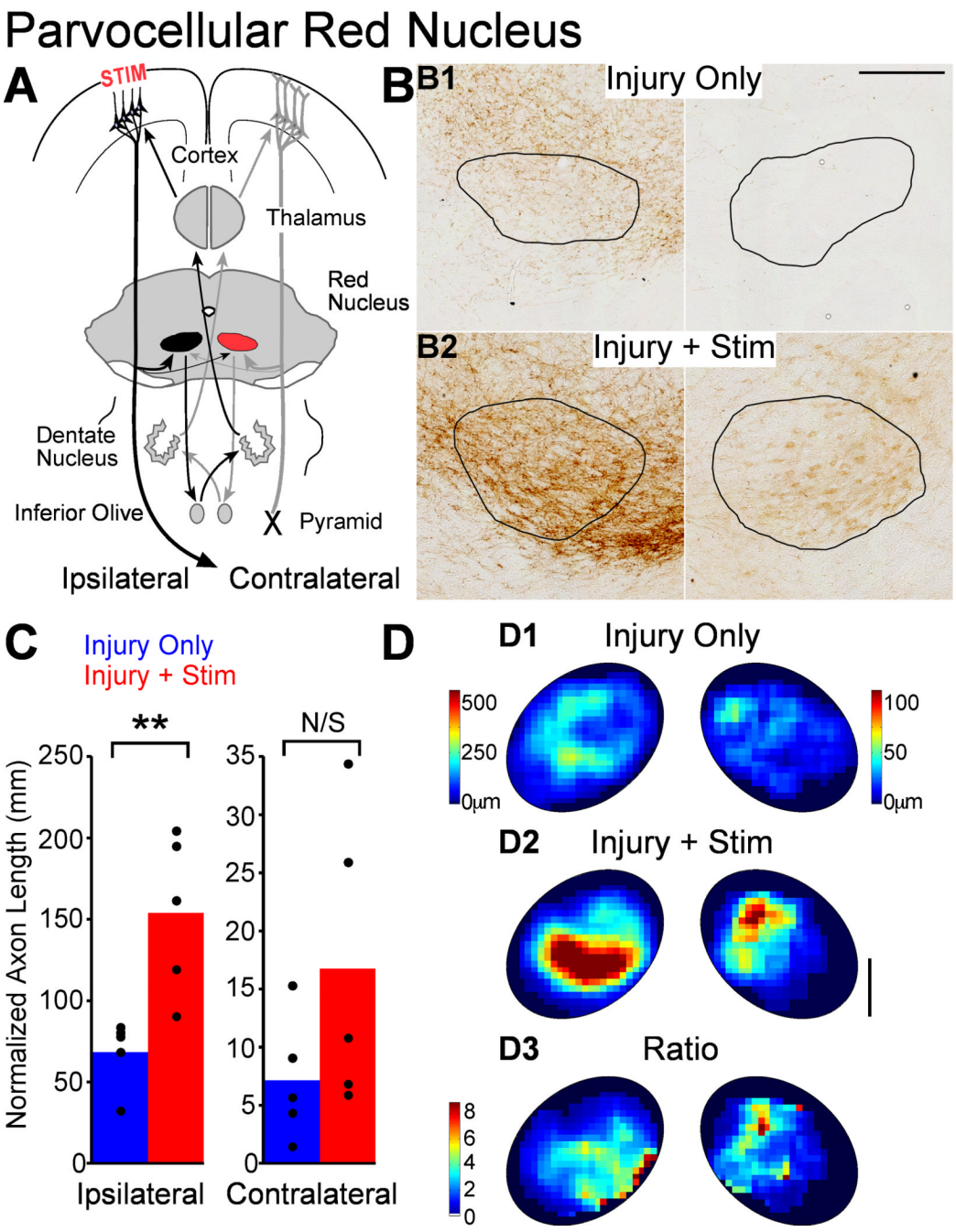

Figure 8.

M1 stimulation causes robust outgrowth to the parvocellular red nucleus. A. Schema. M1 projections to the contralateral nucleus (colored red) could participate in control of the impaired forelimb through a double crossed connection. B. Micrographs of BDA-labeled axons in parvocellular red nucleus (outlined) of representative rats. Scale bar, 250μm. C. Quantification of total axon length. D. Local axon length maps. Intensity scales in D1 also apply to D2. Note the axon length scales are different on the two sides to show the full range on each side. D3. Stimulation-induced outgrowth is shown as the pixel-by-pixel ratio of injury and stimulation rats to injury only rats expressed as fold-change. Scale bar 250μm. * $P<0.05$, corrected for multiple comparisons.

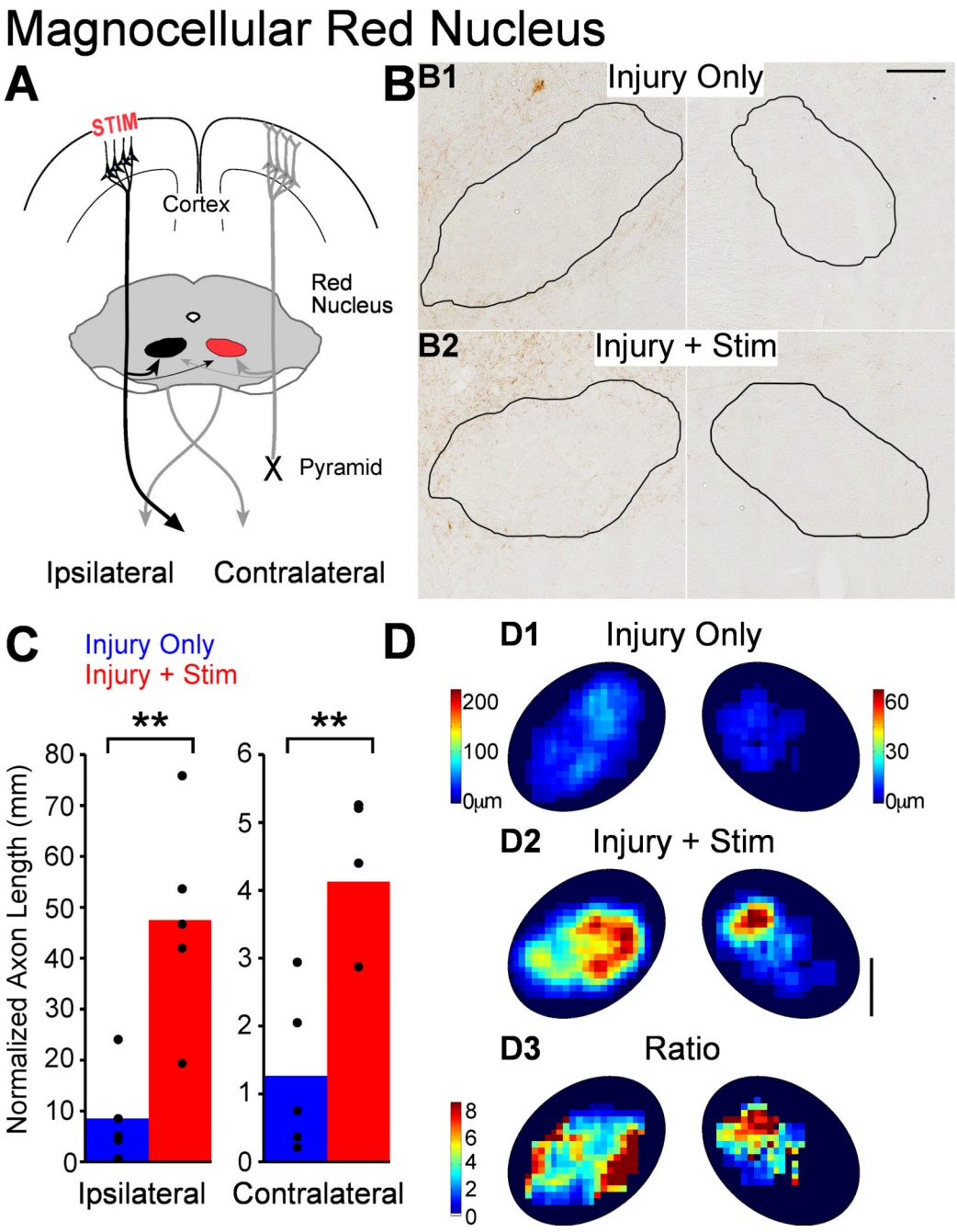

Figure 9.

M1 stimulation causes robust outgrowth to the magnocellular red nucleus. A. Schema. Outgrowth to the contralateral nucleus (colored red) could improve motor control on the impaired side through the re-crossed rubrospinal tract. B. Micrographs of BDA-labeled axons in magnocellular red nucleus (outlined) of representative rats. C. Quantification of total axon length within each red nucleus. Scale bar, 250μm. D. Local axon length maps. Intensity scales in D1 also apply to D2. Note the axon length scales are different on the two sides to show the full range on each side. D3. Stimulation-induced outgrowth is shown as the pixel-by-pixel ratio of injury and stimulation rats to injury only rats expressed as fold-change. Scale bar 250μm. * $P<0.05$, corrected for multiple comparisons.